Anal Bioanal Chem (2017) 409:6227–6234
DOI 10.1007/s00216-017-0563-8

RESEARCH PAPER

Gold nanoparticle-based localized surface plasmon immunosensor for staphylococcal enterotoxin A (SEA) detection

Maroua Ben Haddada[1,2] · David Hu[1] · Michèle Salmain[2] · Lu Zhang[1,3,4] · Chen Peng[3] · Yi Wang[3] · Bo Liedberg[3] · Souhir Boujday[1,4]

Received: 4 April 2017 / Revised: 7 July 2017 / Accepted: 2 August 2017 / Published online: 16 August 2017

Abstract We describe the engineering of stable gold nanoparticle (AuNP) bioconjugates for the detection of staphylococcal enterotoxin A (SEA) using localized surface plasmon resonance (LSPR). Two types of AuNP bioconjugates were prepared by covalently attaching anti-SEA antibody (Ab) or SEA to AuNPs. This was achieved by reacting Traut's reagent with lysine residues of both proteins to generate thiol groups that bind to gold atoms on the AuNP surface. These bioconjugates were characterized in-depth by absorption spectroscopy, cryo-transmission electron microscopy, dynamic light scattering, and zeta potential measurements. Their stability over time was assessed after 1 year storage in the refrigerator at 4 °C. Two formats of homogeneous binding assays were set up on the basis of monitoring of LSPR peak shifts resulting from the immunological reaction between the (i) immobilized antibody and free SEA, the direct assay, or (ii) immobilized SEA and free antibody, the competitive assay. In both formats, a correlation between the LSPR band shift and SEA concentration could be established. Though the competitive format did not meet the expected analytical performance, the direct format, the implementation of which was very simple, afforded a specific and sensitive response within a broad dynamic range—nanogram per milliliter to microgram per milliliter. The limit of detection (LOD) of SEA was estimated to equal 5 ng/mL, which was substantially lower than the LOD obtained using a quartz crystal microbalance. Moreover, the analytical performance of AuNP-Ab bioconjugate was preserved after 1 year of storage at 4 °C. Finally, the LSPR biosensor was successfully applied to the detection of SEA in milk samples. The homogeneous nanoplasmonic immunosensor described herein provides an attractive alternative for stable and reliable detection of SEA in the nanogram per milliliter range and offers a promising avenue for rapid, easy to implement, and sensitive biotoxin detection.

Keywords Immunosensor · Localized surface plasmon resonance · Staphylococcal enterotoxin A · Gold nanoparticles

Introduction

Biotoxins are species produced by microorganisms (bacteria, microalgae) for various purposes. Ingestion of food contaminated by these microorganisms causes various diseases that can, in the worst case, be fatal to humans. For instance, some strains of *Staphylococcus aureus* produce enteroxins that, when ingested, induce severe gastroenteritis mainly caused by the most frequently encountered enterotoxin serotype, namely, staphylococcal enterotoxin A (SEA) [1, 2]. Therefore, control of food safety all along the production chain is necessary to prevent food poisoning outbreaks. Classical analytical methods to detect biotoxins in food samples are generally time-consuming, require highly trained staff

Electronic supplementary material The online version of this article (doi:10.1007/s00216-017-0563-8) contains supplementary material, which is available to authorized users.

✉ Souhir Boujday
souhir.boujday@upmc.fr

[1] UPMC Univ Paris 6, CNRS, Laboratoire de Réactivité de Surface (LRS), Sorbonne Universités, 4 Place Jussieu, 75005 Paris, France

[2] UPMC Univ Paris 06, CNRS, Institut Parisien de Chimie Moléculaire (IPCM), Sorbonne Universités, 4 place Jussieu, 75005 Paris, France

[3] Centre for Biomimetic Sensor Science, School of Material Science and Engineering, Nanyang Technological University, Nanyang 637553, Singapore

[4] MajuLab, UMI 3654, CNRS-UNS-NUS-NTU International Joint Research Unit, Nanyang, Singapore

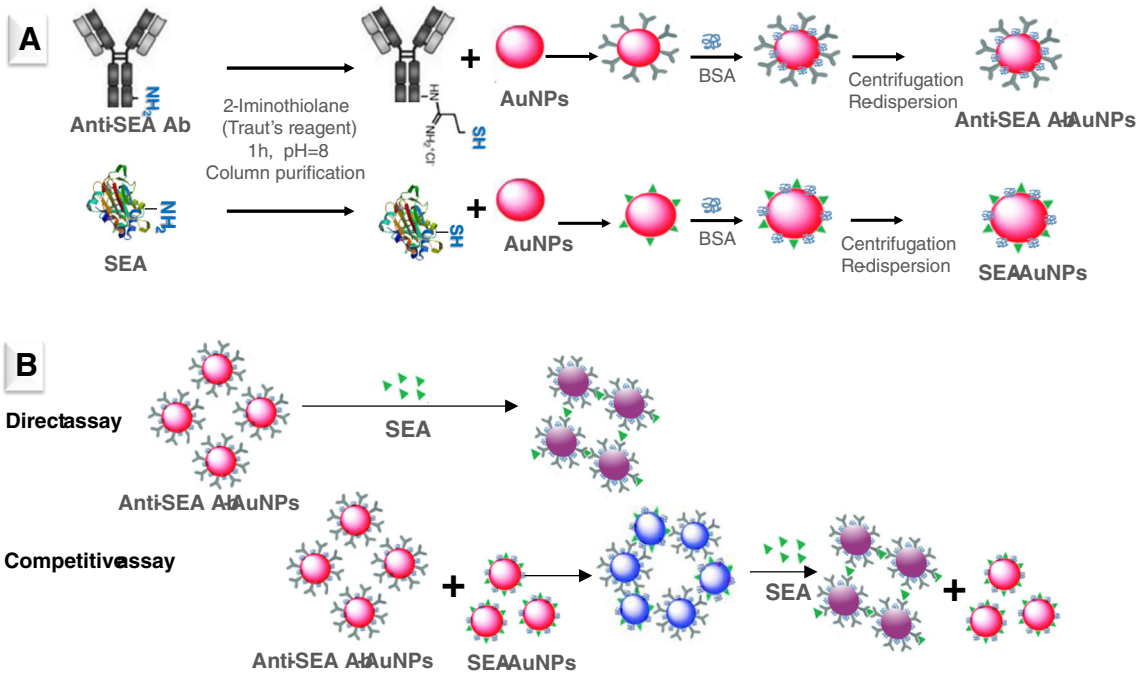

Fig. 1 **A** Adopted strategy for bioconjugates elaboration. **B** Principle of direct and competitive assays

Finally, the biofunctionalized AuNPs were pelleted by centrifugation at 13000 g for 15 min, washed twice to remove unbound and loosely bound Ab and finally resuspended in PBS (3 mL). The concentration of antibody in the first supernatant was assayed by ELISA to estimate the number of Ab bound to AuNPs (see Electronic Supplementary Material (ESM) for experimental details and calculations). The same procedure was applied to prepare AuNP-SEA bioconjugate using a solution of thiolated SEA at 24 μg/mL.

SEA immunosensing In the direct assay, aliquots of SEA stock solution (6 μL of a 0.1 mg/mL or 1 μg/mL solution in water) were serially added to the AuNP-Ab bioconjugate solution (600 μL, OD_{530} = 0.6) in a plastic cuvette. Absorption spectra of the mixtures were measured in real time (millisecond temporal resolution and 10^{-2} nm spectral resolution) using Insplorion XNano II instrument until equilibrium was reached (~ 60 min). The same procedure was used for the competitive assay except that SEA was replaced by AuNP-SEA bioconjugate. The position of the LSPR band was plotted as a function of time using the software provided with the instrument. Error bars are determined experimentally based on a set of a minimum of three assays.

Milk sample preparation and analysis Skimmed milk was reconstituted by dissolving 5 g of powder milk in 9.5 mL water. The pH of the solution was slowly brought to 4.6 by addition of 1 M HCl to precipitate casein, and the suspension was centrifuged at 2550 g for 40 min. The supernatant was collected and the pH was slowly brought to 7 by addition of 1 M NaOH. The suspension was centrifuged at 10000 g for 20 min, and the resulting supernatant (whey fraction) was spiked with 2 μg/mL SEA. Sample (300 μL) was mixed with AuNP-Ab solution (300 μL, OD_{530} = 1) in a plastic cuvette, and the absorption spectrum was recorded every 15 min for up to 95 min on a UV-visible spectrometer (Cary 50, Varian). Mathematical determination of λ_{max} was done according to reference [24].

Results and discussion

Bioconjugate engineering Citrate-capped gold nanoparticles were first characterized by absorption spectroscopy and transmission electron microscopy (TEM). The resulting data, depicted in the ESM (Fig. S1), show a homogeneous distribution with an average particle size of 13.5 ± 1 nm and an LSPR band centered at 520 nm. The hydrodynamic diameter D_H estimated by DLS was slightly larger, 18 ± 1 nm and the zeta potential equal to −45.3 ± 1 mV in agreement with previously published data for citrate-capped AuNP [25]. AuNP-Ab and AuNP-SEA bioconjugates were engineered according to an original procedure schematized in Fig. 1. This coupling method ensures a covalent immobilization of the protein molecules on the surface of the gold nanoparticles by formation of Au-S bonds [21]. It also enables minimizing the distance between the transducer (AuNP) and the bioreceptor (Ab). Indeed, the ability of gold nanoparticles to sense local refractive index changes via LSPR band shift decays rapidly with distance from the gold surface [4].

After reaction and separation of the AuNP by centrifugation, the amount of unbound Ab in the supernatant was found to be very small (2.2 vs 123 μg in the starting solution) as assayed by ELISA (see ESM), confirming the successful conjugation of Ab to AuNP. The final concentration of anti-SEA antibody in the AuNP-Ab solution was estimated 40 μg/mL, and the Ab to AuNP ratio was estimated around 7 (see ESM for calculation details) which is agreement with antibody size versus nanoparticle size (see ESM Fig. S2 and reference [26]).

Upon covalent attachment of anti-SEA Ab to AuNP, the LSPR band underwent a red-shift of 8 nm (λ_{max} = 528 nm) and an additional shift of 1 nm (λ_{max} = 529 nm) was seen upon further blocking by BSA (Fig. 2). The same trend was observed upon SEA grafting to the nanoparticles. These results are in agreement with previously published data [27]. The shape and width of the LSPR bands indicate a homogeneous distribution of the particle size that was confirmed by cryo-TEM images (see inserts in Fig. 2A). Cryo-TEM images also confirmed the colloidal stability of the bioconjugates as no aggregates appeared. Mathematical treatment of cryo-TEM images showed an average size of 13.3 ± 0.7 nm (n = 15) for AuNP-SEA and 14.2 ± 0.7 (n = 15) nm for AuNP-Ab. The increase of particles size due to the grafted proteins could not be seen by cryo-TEM but was evidenced by DLS measurements as the hydrodynamic diameter of AuNP-Ab and AuNP-SEA increased to 76 ± 1 and 54.6 ± 0.5 nm, respectively (Fig. 2; ESM Table S1). As for citrate-coated gold nanoparticles, the hydrodynamic diameter is likely overestimated as the resulting values are larger than expected from geometrical considerations. Indeed, considering the IgG structure (ref [28] and ESM Fig. S2), the diameter of gold nanoparticles covered by a monolayer of chemisorbed antibodies should be around 50 nm maximum. The zeta potential of AuNP in PBS pH 7.4 also increased from −45.3 to −18.9 mV after conjugation of Ab (see Fig. 2b and ESM Table S1) in agreement with previously reported data [29]. The increase was even larger for AuNP-SEA bioconjugate, −6.3 mV. If the surface of gold particles is fully covered with proteins, the net charge of the conjugate is expected to be close to that of the protein itself [30]. The calculated isoelectric point (pI) of SEA is 6.6 according to the ExPASy database, meaning that the protein should be slightly negatively charged at pH 7.4 in accordance with the Z-potential value given above. The pI of rabbit anti-SEA IgG is unknown, but the purification of rabbit IgG from serum by anion exchange chromatography

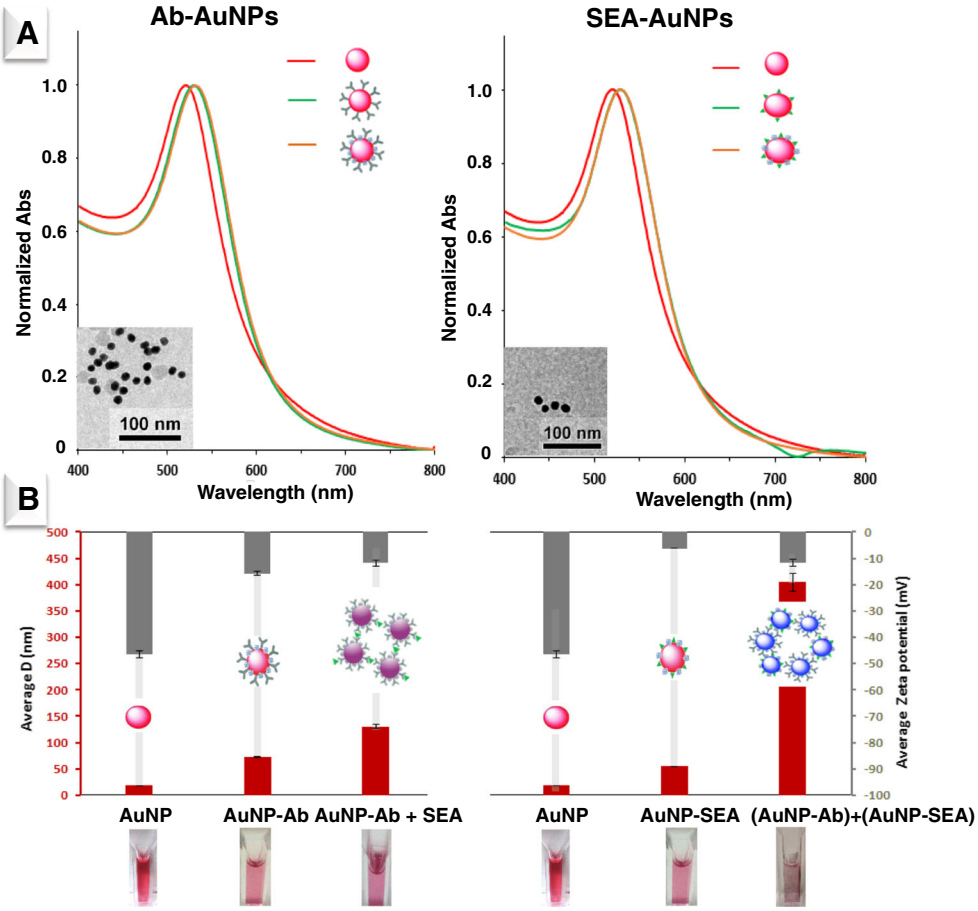

Fig. 2 **A** LSPR band change upon conjugation of anti-SEA Ab (left) and SEA (right) to AuNPs and subsequent BSA backfilling. The inserts show representative cryo-TEM images of AuNP-Ab and AuNP-SEA bioconjugates. **B** Hydrodynamic diameter and zeta potential of citrate-coated AuNP, AuNP conjugates, and mixtures of AuNP-Ab and free SEA or AuNP-SEA conjugate (5 μg/mL). Images or the corresponding solutions are added below

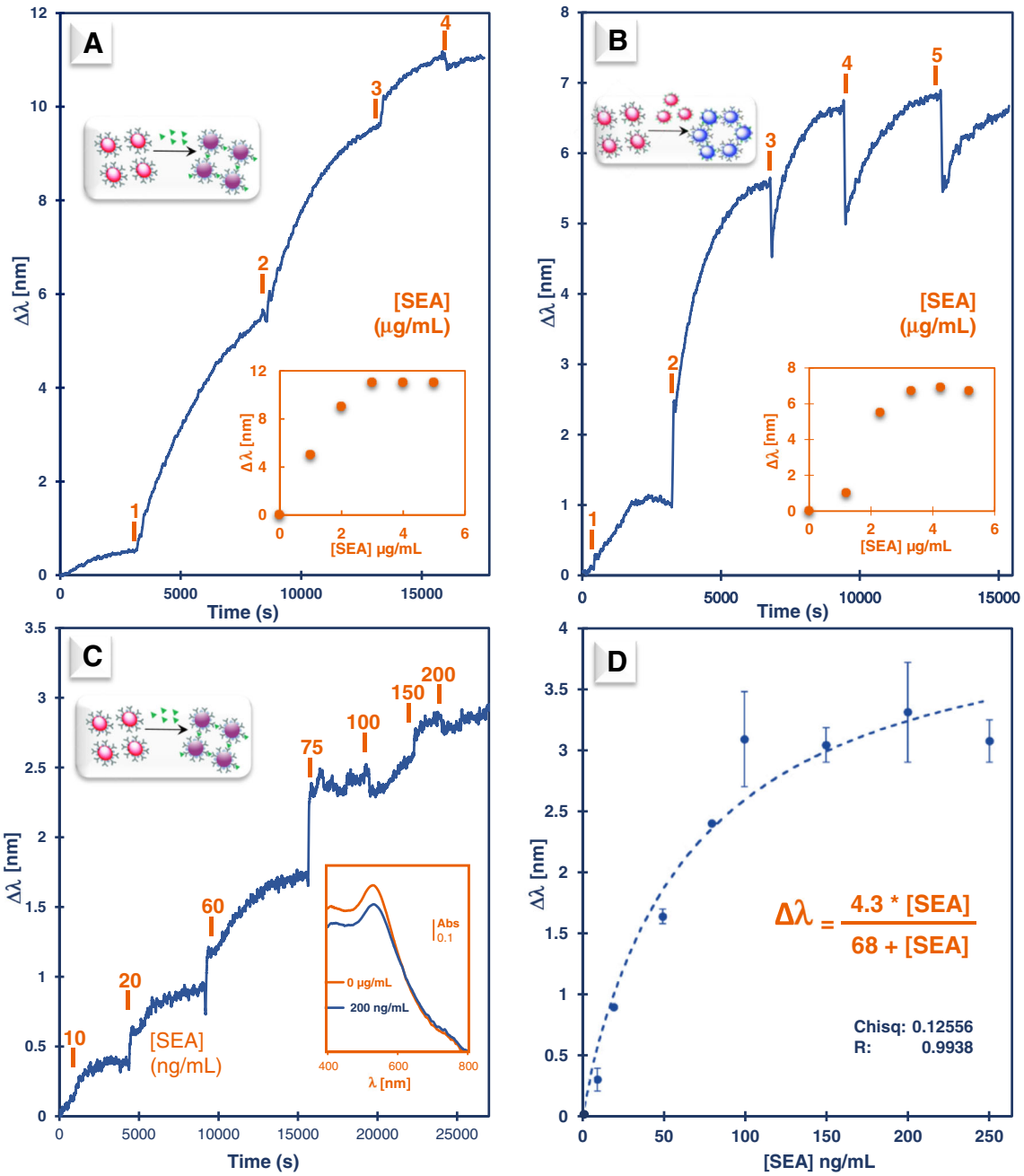

Fig. 3 **A, B** Examples of LSPR curves obtained by incubating AuNP-Ab conjugate with increasing concentrations of free SEA in the 1 to 4 µg/mL range (**A**) and AuNP-SEA (**B**), the inserts show the dose-response curves obtained by plotting the LSPR band shift Δλ as a function of SEA concentration measured after ca. 1 h incubation. **C** Example of LSPR curve obtained by incubating AuNP-Ab conjugate with increasing concentrations of free SEA in the nanogram per milliliter range. The insert shows the LSPR peak for the initial and final AuNP-Ab conjugate. **D** Dose-response curve obtained by plotting the LSPR band shift Δλ from a set of experiments similar to **c** as a function of SEA concentration in the 0 to 250 ng/mL range measured after 50 min incubation, average data from three experiments

was previously shown to afford two IgG fractions with pI 5.65–8.7 and 5.5–7.1, respectively [31]. The Z-potential value of the AuNP-Ab conjugate indicates that this antibody is more negatively charged than SEA at pH 7.4, meaning that its pI is probably below 6, that is in the lower range of the intervals given above. To estimate the Z-potential of the anti-SEA Ab, we measured the zeta potential of a rabbit IgG. The resulting value, −16.1 mV, was in agreement with the zeta potential measured for AuNP-Ab bioconjugate.

In a preliminary experiment, the position of the LSPR band of the colloidal solution of AuNP-Ab was monitored over time upon addition of SEA (1 µg/mL). Progressive shift of the LSPR band to the red Δλ = 5 nm was seen in approx. 1 h (Fig. 3A). Further additions of SEA led to further shifts of the LSPR

band which reached a total shift of $\Delta\lambda$ = 11 nm upon exposure to 3 μg/mL SEA; no further shift was observed for higher SEA concentrations (Fig. 3A and insert therein). In parallel, the hydrodynamic diameter reached 131 nm and the Z-potential shifted form −18.9 to −11.8 mV (Fig. 2B and ESM Table S1).

The same experiment was carried out with AuNP-SEA instead of free SEA. Similarly, progressive shift of the LSPR band to the red was noticed reaching $\Delta\lambda$ = 7 nm at saturation (Fig. 3B). In this case, a perceptible change in color from pink to purple was observed (Fig. 2B, right) as well as a significant increase of the absorbance between 600 and 700 nm (ESM Fig. S3) and a measured average D_H of 404 nm by DLS (Fig. 2B and ESM Table S1). All these data are consistent with the formation of aggregates resulting from interparticle cross-linking through Ab/Ag interactions. In the envisioned competitive detection assay (see Fig. 1), the presence of SEA in the milieu was expected to lead to a "de-aggregation" by breaking the Ab/Ag cross-linking through a competition between free SEA molecules and AuNP-SEA. Unfortunately, addition of free SEA to the mixture of AuNP-Ab and AuNP-SEA did not break the Ab/Ag cross-linking nor lead to particle dispersion as expected [32, 33]. Instead, further shifts of the LSPR band to the red occurred ($\Delta\lambda$=2 nm for [SEA] = 1 μg/mL and $\Delta\lambda$=3.7 nm for [SEA] = 2 μg/mL) possibly because all the available antibody binding sites were not occupied by the antigen from AuNP-SEA in the first place. Extension of the incubation time or change of the AuNP-Ab/AuNP-SEA proportion did not improve the results. We thus conclude that the competitive assay format is not feasible for SEA detection. In what follows, we explore the efficiency of AuNP-Ab in the one-step colorimetric assay of SEA in the direct format depicted in Fig. 1.

Optimizing the homogeneous assay of SEA Since the Insplorion XNano II instrument employed for the LSPR measurements displays high spectral resolution (0.01 nm), we anticipated that much lower band shifts corresponding to lower analyte concentrations could be monitored. Real–time monitoring of the LSPR band position was undertaken upon addition of increasing amounts of SEA in the range 10 to 250 ng/mL (Fig. 3C). A progressive shift of the LSPR band was observed and a dose-response curve was established by plotting the band shift Δλ measured after stabilization (approx. 1 h) versus the concentration of analyte (Fig. 3D). We also used DLS to explore whether it could provide analytical data on SEA detection. DLS results are shown in the ESM, Fig. S4. Though the addition of SEA to the bioconjugate led to a perceptible increase in the hydrodynamic diameter starting from low SEA concentrations (ΔD_H = 50 nm for 10 ng/mL) no consistent change could be observed upon adding higher amounts of SEA; the average hydrodynamic diameter was barely changed after the first addition.

Mathematical fitting of the dose-response curve in Fig. 3D using the Langmuir isotherm equation gave an apparent dissociation constant K_D of 68 ± 13 ng/mL = 2.5 ± 0.5 nM. Therefore, anti-SEA maintained a high affinity for its target after conjugation. The limit of detection was calculated to equal 5 ng/mL = 0.2 nM from 3× the response of a blank sample ($\Delta\lambda$ = 0.1 nm). The dynamic range was widened, and the assay sensitivity was improved as compared to our recently reported piezoelectric immunosensor for SEA [34, 35]; In the direct assay format, using the same antibody reagent and a temperature-controlled quartz crystal microbalance platform, the LOD was 4 times higher, 20 ng/mL. We expect that the limit of detection may be further decreased by replacing the gold nanospheres by nonspherical gold nanoparticles that show higher refractive index sensitivity [4]. It is important to note at this stage that the presence of a plateau in dose-response curve observed in Fig. 2D is surprising if we consider the sensor response at higher SEA concentration plot in Fig. 2D with a higher saturation coverage. This might look controversial and our main hypothesis to explain this

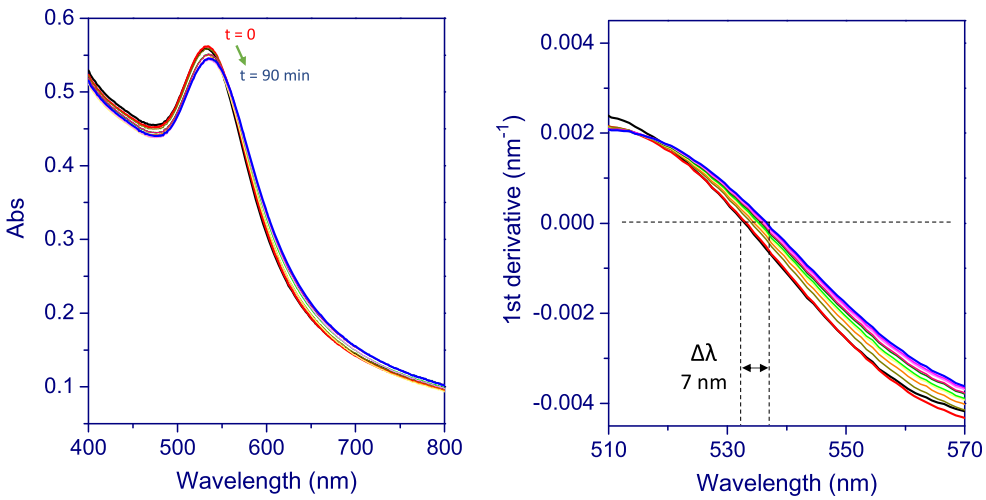

Fig. 4 Left: LSPR curves measured upon incubation of AuNP-Ab conjugate with unspiked milk (black trace) and at increasing incubation time (from 0 to 90 min) with 1 μg/mL SEA in milk (red to blue curves). Right: The first derivatives of the LSPR curves

observation is that there would be two working ranges of the sensor: In the first one, at low SEA concentrations (up to 250 ng/mL), we measure a small shift upon SEA binding to AuNP-Ab bioconjugates. Within this format, we reach a first plateau in the detection mode around 3 nm. At higher SEA concentrations (above 1 μg/mL) the shift is higher and possibly ascribable to AuNP-Ab cross-linking through simultaneous recognition of SEA molecules by antibodies belonging to different bioconjugates; a sort of self-assembly of colloids through Ab/Ag interactions. We envision several experiments to explore this hypothesis, including cryo-TEM analysis at different analyte concentrations in upcoming work.

The same binding experiment performed by addition of 100 up to 2300 ng/mL bovine ß-lactoglobulin (a protein present in high concentration in the whey fraction of cow's milk) to the colloidal solution of AuNP-Ab did not lead to any significant change of the LSPR band (ESM Fig. S5), indicating that previous band shifts were indeed related to the highly selective binding of SEA to anti-SEA conjugated to AuNP.

We assessed the long-term stability of the AuNP-Ab bioconjugate. The same batch of AuNP-Ab bioconjugate, stored in the refrigerator at 4 °C for 1 year was used to reproduce the LSPR experiments for direct detection of SEA. The suspension was visibly stable under storage period and the UV-visible spectra were identical to the original ones confirming that no aggregation occurred (ESM Fig. S6). Note that when antibodies are simply physisorbed on gold nanoparticles, aggregation occurred within less than 2 weeks. The results of LSPR assay of SEA after extended storage are shown in the ESM, Fig. S6. The response of the sensor was similar to the freshly prepared bioconjugate showing a remarkable stability over time paving the way for a commercial use of the developed biosensor.

Finally, the nanoplasmonic immunosensor was applied to the detection of SEA spiked in milk. The absorption spectra obtained upon mixing AuNP-Ab with milk samples (whey fraction) spiked with SEA for increasing incubation time (0 to 90 min) are shown in Fig. 4. These spectra were obtained using benchtop UV-visible spectrometer, nevertheless an obvious shift is observed upon incubation with spiked compared to unspiked milk: The unspiked milk sample gave a λ_{max} = 531 nm whereas the milk sample spiked with 1 μg/mL SEA gave a λ_{max} = 535 nm in good agreement with data obtained in buffer.

To improve the precision of this measurement, we determined λ_{max} following the zero value of the first derivatives of these spectra also shown (in Fig. 4). This methods described in reference [24] allowed us to measure a 7 nm shift at equilibrium. Following these promising preliminary results in milk, the analytical performances of these gold nanoparticle-antibody bioconjugates in food matrices will be deeply investigated in future work.

Conclusions

Stable gold nanoparticle-antibody bioconjugate (AuNP-Ab) was engineered by covalently linking anti-SEA antibody to citrate-capped gold nanoparticles using Traut's reagent. This bioconjugate was studied in-depth by several characterization techniques and was remarkably stable after 1 year storage in the refrigerator at 4 °C. Two formats of homogeneous binding assays of staphylococcal enterotoxin A (SEA) by localized surface plasmon resonance (LSPR) were set up based on a direct assay strategy, in which AuNP-Ab was reacted with SEA, and a competitive assay starting from a mixture of AuNP-Ab and AuNP-SEA bioconjugates. Correlation between plasmon shifts and SEA concentration was established when the anti-SEA antibody conjugated to AuNP was mixed with SEA in the free form or conjugated to AuNP. In the case of mixtures AuNP-Ab and AuNP-SEA bioconjugates (competitive format), a red-shift of the plasmon peak along with nanoparticle aggregation were observed. However, addition of free SEA to the mixture of AuNP-Ab and AuNP-SEA did not lead to particle dispersion suggesting that this competitive format is not feasible for SEA assay. The one-step LSPR assay of SEA with AuNP-Ab bioconjugate afforded remarkable analytical performances at the ng/mL level. SEA was assayed in both the ng/mL and μg/mL working ranges with a calculated limit of detection (LOD) of 5 ng/mL (0.2 nM). Moreover, the response of the sensor after 1 year storage at 4 °C was similar to the freshly prepared bioconjugate showing a remarkable stability over time. Preliminary assays in spiked milk confirmed the efficiency of these bioconjugates for SEA biosensing in food matrix. The nanoplasmonic immunosensor described herein requires rather simple optical equipment and straightforward manipulations, and provides an attractive alternative to more bulky and expensive approaches for rapid and sensitive detection of SEA and other toxins.

Acknowledgements We would like to thank the DIM Analytics and Region Ile-de-France for M. Ben Haddada PhD scholarship. We also thank Anton Paar for the access to Litesizer™ 500 apparatus. This work was supported by the iFood initiative Nanyang Technological University, by the French-Singaporean PHC Merlion program (grant 5.03.15), and by the ANR-FWF program (grant ANR-15-CE29-0026).

Compliance with ethical standards

Conflict of interest The authors declare that they have no competing interests.

References

1. Hennekinne J-A, De Buyser M-L, Dragacci S. Staphylococcus aureus and its food poisoning toxins: characterization and outbreak investigation. FEMS Microbiol Rev. 2012;36:815–36.

2. Le Loir Y, Baron F, Gautier M. Staphylococcus aureus and food poisoning. Genet Mol Res. 2003;2(1):63–76.
3. Jans H, Huo Q. Gold nanoparticle-enabled biological and chemical detection and analysis. Chem Soc Rev. 2012;41(7):2849–66. doi:10.1039/C1CS15280G.
4. Mayer KM, Hafner JH. Localized surface plasmon resonance sensors. Chem Rev. 2011;111(6):3828–57. doi:10.1021/cr100313v.
5. Sepulveda B, Angelome PC, Lechuga LM, Liz-Marzan LM. LSPR-based nanobiosensors. Nano Today. 2009;4(3):244–51. doi:10.1016/j.nantod.2009.04.001.
6. Rong-Hwa S, Shiao-Shek T, Der-Jiang C, Yao-Wen H. Gold nanoparticle-based lateral flow assay for detection of staphylococcal enterotoxin B. Food Chem. 2010;118(2):462–6. doi:10.1016/j.foodchem.2009.04.106.
7. Wang WB, Liu LQ, Xu LG, Kuang H, Zhu JP, Xu CL. Gold-nanoparticle-based multiplexed immunochromatographic strip for simultaneous detection of staphylococcal enterotoxin A, B, C, D, and E. Part Part Syst Charact. 2016;33(7):388–95. doi:10.1002/ppsc.201500219.
8. Englebienne P. Use of colloidal gold surface plasmon resonance peak shift to infer affinity constants from the interactions between protein antigens and antibodies specific for single or multiple epitopes. Analyst. 1998;123(7):1599–603. doi:10.1039/A804010I.
9. Mayer KM, Lee S, Liao H, Rostro BC, Fuentes A, Scully PT, et al. A label-free immunoassay based upon localized surface plasmon resonance of gold Nanorods. ACS Nano. 2008;2(4):687–92. doi:10.1021/nn7003734.
10. Nath N, Chilkoti A. Label-free biosensing by surface plasmon resonance of nanoparticles on glass: optimization of nanoparticle size. Anal Chem. 2004;76(18):5370–8. doi:10.1021/ac049741z.
11. Liu XH, Wang Y, Chen P, Wang YS, Mang JL, Aili D, et al. Biofunctionalized gold nanoparticles for colorimetric sensing of Botulinum neurotoxin A light chain. Anal Chem. 2014;86(5):2345–52. doi:10.1021/ac402626g.
12. Zhao W, Brook MA, Li Y. Design of Gold Nanoparticle-Based Colorimetric biosensing assays. Chembiochem. 2008;9(15):2363–71. doi:10.1002/cbic.200800282.
13. Montenegro J-M, Grazu V, Sukhanova A, Agarwal S, de la Fuente JM, Nabiev I, et al. Controlled antibody/(bio-) conjugation of inorganic nanoparticles for targeted delivery. Adv Drug Deliv Rev. 2013;65(5):677–88. doi:10.1016/j.addr.2012.12.003.
14. Wang Z, Ma L. Gold nanoparticle probes. Coord Chem Rev. 2009;253(11–12):1607–18. doi:10.1016/j.ccr.2009.01.005.
15. Wang X, Mei Z, Wang Y, Tang L. Comparison of four methods for the biofunctionalization of gold nanorods by the introduction of sulfhydryl groups to antibodies. Beilstein J Nanotechnol. 2017;8:372–80. doi:10.3762/bjnano.8.39.
16. Boujday S, Bantegnie A, Briand E, Marnet P-G, Salmain M, Pradier C-M. In-depth investigation of protein adsorption on gold surfaces: correlating the structure and density to the efficiency of the sensing layer. J Phys Chem B. 2008;112(21):6708–15.
17. Wang X, Mei Z, Wang Y, Tang L. Gold nanorod biochip functionalization by antibody thiolation. Talanta. 2015;136:1–8. doi:10.1016/j.talanta.2014.11.023.
18. Slot JW, Geuze HJ. A method to prepare isodisperse colloidal gold sols in the size range 3–17 NM. Ultramicroscopy. 1984;15(4):383. doi:10.1016/0304-3991(84)90144-X.
19. Ben Haddada M, Huebner M, Casale S, Knopp D, Niessner R, Salmain M, et al. Gold nanoparticles assembly on silicon and gold surfaces: mechanism, stability, and efficiency in diclofenac biosensing. J Phys Chem C. 2016;120:29302–11.
20. Dixit CK, Kaushik A. Nano-structured arrays for multiplex analyses and lab-on-a-chip applications. Biochem Biophys Res Commun. 2012;419(2):316–20. doi:10.1016/j.bbrc.2012.02.018.
21. Sule Shantanu V, Sukumar M, Weiss William F IV, Marcelino-Cruz Anna M, Sample T, Tessier Peter M. High-throughput analysis of concentration-dependent antibody self-association. Biophys J. 2011;101(7):1749–57. doi:10.1016/j.bpj.2011.08.036.
22. Hermanson GT. Chapter 1—functional targets. In: bioconjugate techniques. Second ed. New York: Academic Press; 2008. p. 1–168. doi:10.1016/B978-0-12-370501-3.00001-1.
23. Hermanson GT. Chapter 24—Preparation of colloidal gold-labeled proteins. In: Hermanson GT, editor. Bioconjugate techniques. Second ed. New York: Academic Press; 2007. p. 924–35. doi:10.1016/B978-0-12-370501-3.00024-2.
24. Chen P, Liedberg B. Curvature of the localized surface plasmon resonance peak. Anal Chem. 2014;86(15):7399–405. doi:10.1021/ac500883x.
25. Xia H, Xiahou Y, Zhang P, Ding W, Wang D. Revitalizing the Frens method to synthesize uniform, quasi-spherical gold nanoparticles with deliberately regulated sizes from 2 to 330 nm. Langmuir. 2016;32(23):5870–80. doi:10.1021/acs.langmuir.6b01312.
26. Sperling RA, Parak WJ. Surface modification, functionalization and bioconjugation of colloidal inorganic nanoparticles. Philos Trans R Soc A Math Phys Eng Sci. 2010;368(1915):1333–83. doi:10.1098/rsta.2009.0273.
27. Thobhani S, Attree S, Boyd R, Kumarswami N, Noble J, Szymanski M, et al. Bioconjugation and characterisation of gold colloid-labelled proteins. J Immunol Methods. 2010;356(1–2):60–9. doi:10.1016/j.jim.2010.02.007.
28. Klein JS, Gnanapragasam PNP, Galimidi RP, Foglesong CP, West AP, Bjorkman PJ. Examination of the contributions of size and avidity to the neutralization mechanisms of the anti-HIV antibodies b12 and 4E10. Proc Natl Acad Sci. 2009;106(18):7385–90. doi:10.1073/pnas.0811427106.
29. Hinterwirth H, Stübiger G, Lindner W, Lämmerhofer M. Gold nanoparticle-conjugated anti-oxidized low-density lipoprotein antibodies for targeted Lipidomics of oxidative stress biomarkers. Anal Chem. 2013;85(17):8376–84. doi:10.1021/ac401778f.
30. Yang WJ, Trau D, Renneberg R, Yu NT, Caruso F. Layer-by-layer construction of novel biofunctional fluorescent microparticles for immunoassay applications. J Colloid Interface Sci. 2001;234(2):356–62. doi:10.1006/jcis.2000.7325.
31. Geoghegan WD. The effect of three variables on adsorption of rabbit IgG to colloidal gold. J Histochem Cytochem. 1988;36(4):401–7. doi:10.1177/36.4.3346540.
32. Liu X, Huo Q. A washing-free and amplification-free one-step homogeneous assay for protein detection using gold nanoparticle probes and dynamic light scattering. J Immunol Methods. 2009;349(1–2):38–44. doi:10.1016/j.jim.2009.07.015.
33. Tsai CS, Yu TB, Chen CT. Gold nanoparticle-based competitive colorimetric assay for detection of protein-protein interactions. Chem Commun. 2005;34:4273–5. doi:10.1039/b507237a.
34. Salmain M, Ghasemi M, Boujday S, Pradier CM. Elaboration of a reusable immunosensor for the detection of staphylococcal enterotoxin A (SEA) in milk with a quartz crystal microbalance. Sens Actuator B Chem. 2012;173:148–56. doi:10.1016/j.snb.2012.06.052.
35. Salmain M, Ghasemi M, Boujday S, Spadavecchia J, Techer C, Val F, et al. Piezoelectric immunosensor for direct and rapid detection of staphylococcal enterotoxin A (SEA) at the ng level. Biosens Bioelectron. 2011;29(1):140–4. doi:10.1016/j.bios.2011.08.007.